J. Fluid Mech. (1988), *vol.* 188, *pp.* 547–570
Printed in Great Britain

Thermal convection during the directional solidification of a pure liquid with variable viscosity

By MARC K. SMITH

Department of Mechanical Engineering, The Johns Hopkins University, Baltimore, MD 21218, USA

(Received 31 March 1987 and in revised form 4 August 1987)

The onset of a buoyancy-driven instability during the directional solidification of a pure liquid with a strongly temperature-dependent viscosity and an arbitrary Prandtl number is investigated using linear stability theory. The Rayleigh number for this system contains the lengthscale L_s defined as the ratio of the thermal diffusivity of the liquid and the solidification velocity times the density ratio of the two phases. It is independent of the actual depth of the liquid and it reflects the fact that increasing the solidification velocity stabilizes the system. The theory also shows that the difference in material properties between the two phases and the properties of the solidifying interface itself cause the interface to look like a boundary of finite conductivity measured by a wavenumber-dependent Biot number. For large viscosity variations, convection occurs below a stagnant layer which forms just beneath the interface where the liquid is immobilized by its very large viscosity. The thickness of this layer is measured by the natural logarithm of the viscosity contrast in the liquid times the lengthscale L_s. In this limit, the influence of the solidifying boundary is shielded from the bulk liquid by the stagnant layer and so the effect of the Biot number on the critical Rayleigh number is small. However, inertial effects, being associated with the *bulk* liquid, are very important for small Prandtl numbers of the fluid far from the interface. The model has applications to the solidification of magma chambers or lava lakes and to the material processing of polymeric liquids.

1. Introduction

The influence of thermal convection on various processes in geophysical systems has been studied appreciably for the past couple of decades. It has been shown to be of importance in determining the temperature field in the Earth's mantle, in supplying the energy needed for continental drift, and in determining the rate of cooling and the crystallization structure of large magma chambers in the Earth's interior. The simplest estimates for the magnitude of thermal convection in these systems use the model proposed by Lord Rayleigh (1916). In this model, a liquid layer of constant viscosity and thickness is heated from below. Rayleigh's results and the results of others on this system are well reviewed by Chandrasekhar (1961). Briefly, we know that the system will undergo convective overturning when the dimensionless Rayleigh number, a ratio of buoyancy forces to viscous forces, exceeds a critical value that depends on the boundary conditions.

Our primary interest is the cooling of large magma chambers in the Earth's

interior or the cooling of large lava lakes on the Earth's surface. Using the simple liquid-layer convection model on these systems is inappropriate for the following reasons. First, magma is not a constant-viscosity liquid, as shown by Shaw *et al.* (1968). Secondly, the temperature field in the magma is *unsteady* owing to the cooling process, and thirdly, the depth of the layer may not be the same as the lengthscale of the convection. Some of the recent research in this area has been aimed at correcting these deficiencies.

The first of these concerns has been addressed in the experiments of Booker (1976), Richter, Nataf & Daly (1983), Oliver & Booker (1983), and the theory and experiments of Stengel, Oliver & Booker (1982). The results of the theoretical work, which used a fluid whose viscosity depended exponentially on the temperature, are as follows. As the viscosity contrast between top and bottom increases, the critical Rayleigh number initially increases, reaches a maximum, and then decreases monotonically. The wavenumber initially increases or decreases depending on the boundary conditions, but eventually it always increases monotonically with viscosity contrast. The simple physical explanation for this behaviour, discussed by Stengel *et al.* (1982), is that for large enough viscosity contrasts across the layer, a stagnant layer develops at the top and convection occurs in a sublayer at the bottom. The thickness of this sublayer decreases with increasing viscosity contrast. Thus, if the results are rescaled according to the parameters of this convective sublayer, one finds that the critical Rayleigh number and the critical wavenumber approach constants for large enough viscosity contrasts. This indicates that the parameters of the sublayer are the appropriate scales for the problem in this limit.

The second concern, that of a time-dependent basic state due to cooling of the magma, has been explored in the work of Foster (1965), Currie (1967), Mahler, Schechter & Wissler (1968), Homsy (1973), Jhaveri & Homsy (1982) and Neitzel (1982), to name a few. As reviewed by Homsy (1973), two methods have been used. In the first, the time-dependent basic state is frozen and its stability is investigated using linear theory with time as a parameter. In the second, the linearized disturbance equations are integrated in time subject to some prescribed initial conditions and including the time-dependent basic state. The difficulty here is in defining the onset of the instability. In both methods, the computed results do not agree well with experiments. However, these problems seem to have been overcome in the nonlinear energy theory of Homsy (1973) and Neitzel (1982) and in the statistical work of Jhaveri & Homsy (1982).

In all of the above unsteady work, the liquid was assumed to have a constant viscosity. Recently, Jaupart & Parsons (1985) combined variable viscosity with a time-dependent basic state and integrated the linearized disturbance equations in time. Their results also show the development of a stagnant layer above a convecting sublayer as described earlier in the variable-viscosity, steady-state work. However, their results are still subject to all of the criticisms of the previous unsteady work. In addition, they included viscosity as a function of depth alone, independent of the dynamics of the system. This is an awkward way to address the temperature dependence of viscosity.

The last concern associated with applying thermal convection models to a cooling magma system is that the lengthscale of convection may not be the same as the depth of the fluid layer. We have already seen this in the variable-viscosity work when a stagnant layer develops in the liquid. A similar change in lengthscales can appear owing to a solidification process in the magma. Here, an appropriate lengthscale would be based on thermal diffusion and the convection zone it characterizes would

move along with the developing solidification front. The system never feels the effect of the lower boundary until the upper surface gets sufficiently close to it.

Shvartsblat, as discussed in the book by Gershuni & Zhukhovitskii (1976), crudely modelled this effect by investigating convection in a liquid layer with permeable boundaries in which fluid was injected at the lower boundary and removed at the upper boundary with a constant velocity. At large values of this injection velocity, a boundary-layer-like temperature profile appeared. Shvartsblat showed that in this limit the Rayleigh number and the wavenumber computed with the boundary-layer lengthscale became constant. This indicates that the lower boundary has no effect on the system's instability.

This same boundary-layer behaviour of the basic state has also been seen in directional solidification problems of a binary alloy. The model used in such problems is the solidification of an originally planar interface at a constant velocity into a semi-infinite liquid containing a small concentration of another material. In this system, the solute is rejected at the freezing interface and two types of instabilities become possible. The first is a purely morphological one originally studied by Mullins & Sekerka (1964). The second is a convective instability due to the solute material being lighter than the liquid it is dissolved in. The interaction of these two modes of instablity have been well studied by Coriell *et al.* (1980), Hurle, Jakeman & Wheeler (1982, 1983), McFadden *et al.* (1984), Caroli *et al.* (1985*a*, *b*) and Young & Davis (1986), among others.

In the present work, we shall study a model for the onset of thermal convection in cooling magma systems which combines the essential features of this previous work. The model is the directional solidification of a pure substance with a strongly temperature-dependent viscosity. It addresses the first concern by including variable viscosity. The inherent unsteadiness of the cooling process is taken into account by moving with the solidification interface and assuming that we are far enough away from the initial stages of solidification such that the solidification rate is approximately constant. This assumption is equivalent to finding a time when the rate of change in the solidification rate is much less than the growth rate of the thermal instability. This is like the frozen-time approximation done in the earlier studies of unsteady thermal convection. The last concern is addressed since the pure substance is semi-infinite in extent. Thus, the convection will develop its own lengthscale based on thermal diffusion. The actual depth of the liquid in the cooling magma system does not enter the model. However, we shall compare these two lengthscales to see if our modelling is accurate.

Since the simple directional solidification model has been extremely useful in understanding the processing of binary alloys, we also expect that this model will be quite useful in those areas of materials processing which use polymeric fluids that have a strongly temperature-dependent viscosity.

In §2, we shall formally pose the model and formulate the appropriate linear stability equations for the system. The method of solution of this system is described in §3. The results for a wide variety of system parameters are given in §4. Finally, we discuss the physical meaning of our results and their implication in terms of the cooling from above of a large magma chamber or lava lake.

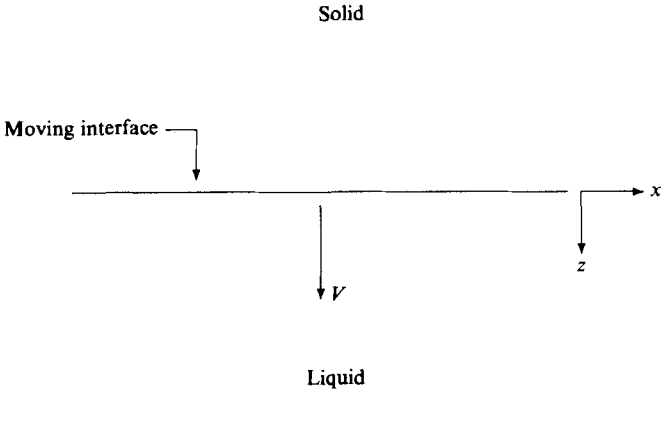

FIGURE 1. A sketch of the solidification model.

2. Problem formulation

In the model shown in figure 1, a pure liquid with a strongly temperature-dependent viscosity is solidifying downward along a planar interface at the fixed velocity V. The governing equations are written with respect to a Cartesian coordinate system fixed in the solid with the z-axis pointing downward. For the solid, we have only conservation of energy,

$$\frac{\partial T_S}{\partial t} = \kappa_S \nabla^2 T_S, \tag{2.1}$$

where T_S is the solid temperature, κ_S is the thermal diffusivity of the solid and t is the time variable. The density of the solid, ρ_S, is also a relevant parameter. For the liquid, we have conservation of energy and mass, and we shall use the Boussinesq approximation in the conservation of momentum equation:

$$\frac{\partial T_L}{\partial t} + \boldsymbol{v}\cdot\boldsymbol{\nabla} T_L = \kappa_L \nabla^2 T_L, \tag{2.2a}$$

$$\boldsymbol{\nabla}\cdot\boldsymbol{v} = 0, \tag{2.2b}$$

$$\rho_L\left\{\frac{\partial \boldsymbol{v}}{\partial t} + (\boldsymbol{v}\cdot\boldsymbol{\nabla})\,\boldsymbol{v}\right\} = -\boldsymbol{\nabla} p + \tilde{\rho}_L g \boldsymbol{e}_3 + \boldsymbol{\nabla}\cdot(\mu_L \boldsymbol{D}), \tag{2.2c}$$

where

$$D_{ij} = v_{i,j} + v_{j,i}, \tag{2.2d}$$

and $\boldsymbol{e}_3$ is a unit vector in the z-direction. The equations of state for the density and viscosity are

$$\tilde{\rho}_L = \rho_L\{1-\beta(T_L - T_0)\}, \tag{2.3a}$$

$$\mu_L = \mu_L(T_L). \tag{2.3b}$$

Here, T_L, $\boldsymbol{v}$ and p, are the liquid temperature, velocity and pressure, and κ_L, ρ_L, μ_L and β are the liquid thermal diffusivity, density, viscosity and thermal-expansion coefficient respectively. Also, T_0 is a reference temperature and g is the acceleration due to gravity.

The interface is located at $z = \eta(x, y, t)$. The normal to the interface is

$$\boldsymbol{n} = (-\eta_x, -\eta_y, 1)(1+\eta_x^2+\eta_y^2)^{-\frac{1}{2}}, \tag{2.4a}$$

the tangential vectors are

$$\boldsymbol{t}^{(1)} = (1, 0, \eta_x)(1+\eta_x^2)^{-\frac{1}{2}}, \tag{2.4b}$$

$$\boldsymbol{t}^{(2)} = (-\eta_x\eta_y, 1+\eta_x^2, \eta_y)(1+\eta_x^2)^{-\frac{1}{2}}(1+\eta_x^2+\eta_y^2)^{-\frac{1}{2}}, \tag{2.4c}$$

and the total curvature of the interface is

$$K = \frac{\eta_{xx}(1+\eta_y^2)+\eta_{yy}(1+\eta_x^2)-2\eta_x\eta_y\eta_{xy}}{(1+\eta_x^2+\eta_y^2)^{\frac{3}{2}}}. \tag{2.4d}$$

If $K < 0$, the interface is convex downward.

The boundary conditions on the interface are continuity of temperature,

$$T_{\mathrm{S}} = T_{\mathrm{S}} = T_{\mathrm{m}}\left(1+K\frac{\gamma}{L}\right), \tag{2.5a,b}$$

where γ is the surface energy at the solid–liquid interface, L is the latent heat per unit volume of the solid and T_{m} is the melting point of the solid; conservation of energy,

$$\boldsymbol{n}\cdot(k_{\mathrm{S}}\nabla T_{\mathrm{S}} - k_{\mathrm{L}}\nabla T_{\mathrm{L}}) = L\eta_t\,\boldsymbol{e}_3\cdot\boldsymbol{n}, \tag{2.5c}$$

where k_{S} and k_{L} are the thermal conductivities of the solid and liquid; conservation of mass,

$$\rho_{\mathrm{L}}\boldsymbol{v}\cdot\boldsymbol{n} = \eta_t\,\boldsymbol{e}_3\cdot\boldsymbol{n}(\rho_{\mathrm{L}}-\rho_{\mathrm{S}}); \tag{2.5d}$$

and the no-slip conditions,

$$\boldsymbol{v}\cdot\boldsymbol{t}^{(1)} = \boldsymbol{v}\cdot\boldsymbol{t}^{(2)} = 0. \tag{2.5e,f}$$

Far away from the interface in the liquid we impose a temperature $T_\infty > T_{\mathrm{m}}$ and also let $|\boldsymbol{v}| < \infty$. Thus, the solidification process is driven by cooling from above.

To simplify the resulting analysis, we make a Galilean transformation and attach a coordinate system to the moving interface. Next, we refer the equations to the following scales: reference temperature T_{m}; temperature difference, $\Delta T = T_\infty - T_{\mathrm{m}}$; velocity, $V_{\mathrm{s}} = V\rho_{\mathrm{S}}/\rho_{\mathrm{L}}$; length, $L_{\mathrm{s}} = \kappa_{\mathrm{L}}/V_{\mathrm{s}}$; time, $t_{\mathrm{s}} = L_{\mathrm{s}}/V_{\mathrm{s}}$; pressure, $P_{\mathrm{s}} = \mu_\infty V_{\mathrm{s}}/L_{\mathrm{s}}$; and viscosity μ_∞, the viscosity at T_∞. We also define $\nu_\infty = \mu_\infty/\rho_{\mathrm{L}}$ and the specific heat of the liquid $c_{\mathrm{L}} = k_{\mathrm{L}}/(\rho_{\mathrm{L}}\kappa_{\mathrm{L}})$.

Our equations reduce to the following:

for the solid,

$$\frac{\partial T_{\mathrm{S}}}{\partial t} - \frac{1}{\rho}\frac{\partial T_{\mathrm{S}}}{\partial z} = \kappa\nabla^2 T_{\mathrm{S}}; \tag{2.6}$$

for the liquid,

$$\frac{\partial T_{\mathrm{L}}}{\partial t} + \boldsymbol{v}\cdot\nabla T_{\mathrm{L}} = \nabla^2 T_{\mathrm{L}}, \tag{2.7a}$$

$$\nabla\cdot\boldsymbol{v} = 0, \tag{2.7b}$$

$$P^{-1}\left\{\frac{\partial\boldsymbol{v}}{\partial t} + (\boldsymbol{v}\cdot\nabla)\,\boldsymbol{v}\right\} = -\nabla p - RT_{\mathrm{L}}\,\boldsymbol{e}_3 + \nabla\cdot(\mu\boldsymbol{D}), \tag{2.7c}$$

$$D_{ij} = v_{i,j} + v_j, i; \tag{2.7d}$$

boundary conditions on $z = \eta$,

$$T_{\mathrm{L}} = T_{\mathrm{S}} = \Gamma K, \tag{2.8a,b}$$

$$\boldsymbol{n}\cdot\{k\nabla T_{\mathrm{S}} - \nabla T_{\mathrm{L}}\} = \mathscr{L}(\rho^{-1}+\eta_t)\,\boldsymbol{e}_3\cdot\boldsymbol{n}, \tag{2.8c}$$

$$\boldsymbol{v}\cdot\boldsymbol{n} = \{(1-\rho)\,\eta_t - 1\}\,\boldsymbol{e}_3\cdot\boldsymbol{n}, \tag{2.8d}$$

$$\boldsymbol{v}\cdot\boldsymbol{t}^{(1)} = -\rho^{-1}\boldsymbol{e}_3\cdot\boldsymbol{t}^{(1)}, \tag{2.8e}$$

$$\boldsymbol{v}\cdot\boldsymbol{t}^{(2)} = -\rho^{-1}\boldsymbol{e}_3\cdot\boldsymbol{t}^{(2)}; \tag{2.8f}$$

boundary conditions on $z \to \infty$,

$$T_{\mathrm{L}} = 1, \quad |\boldsymbol{v}| < \infty. \tag{2.9a,b}$$

Here, all velocities are measured in the moving coordinate system and η is the deviation of the interface from its planar configuration. The dimensionless groups are defined as follows:

$$\kappa = \frac{\kappa_{\mathrm{S}}}{\kappa_{\mathrm{L}}}, \quad \rho = \frac{\rho_{\mathrm{S}}}{\rho_{\mathrm{L}}}, \quad k = \frac{k_{\mathrm{S}}}{k_{\mathrm{L}}},$$

$$P = \frac{\nu_\infty}{\kappa_{\mathrm{L}}}, \qquad \text{the Prandtl number,}$$

$$R = \frac{g\beta\,\Delta T\,\kappa_{\mathrm{L}}^2}{\nu_\infty V^3 \rho^3}, \quad \text{the Rayleigh number,}$$

$$\mathscr{L} = \frac{L}{\rho_{\mathrm{L}} c_{\mathrm{L}} \Delta T}, \quad \text{the Stefan number,}$$

$$\Gamma = \frac{T_{\mathrm{m}} \gamma V}{\Delta T\, L \kappa_{\mathrm{L}}}, \quad \text{the surface-tension number.}$$

Also, $\mu = \mu(T_{\mathrm{L}})$ is the dimensionless viscosity function.

The basic state under consideration is a planar interface moving at the constant speed V. Thus, we have

$$\bar{\boldsymbol{v}} = -\boldsymbol{e}_3, \quad \bar{\eta} = 0, \quad \frac{\mathrm{d}\bar{p}}{\mathrm{d}z} = -R\bar{T}_{\mathrm{L}}. \tag{2.10a,b,c}$$

This simplifies the liquid energy equation to

$$\frac{\mathrm{d}^2\bar{T}_{\mathrm{L}}}{\mathrm{d}z^2} + \frac{\mathrm{d}\bar{T}_{\mathrm{L}}}{\mathrm{d}z} = 0,$$

$$\bar{T}_{\mathrm{L}}(0) = 0, \quad \bar{T}_{\mathrm{L}}(\infty) = 1.$$

Thus,

$$\bar{T}_{\mathrm{L}} = 1 - \mathrm{e}^{-z}. \tag{2.11}$$

The solid energy equation is

$$\rho\kappa \frac{\mathrm{d}^2\bar{T}_{\mathrm{S}}}{\mathrm{d}z^2} + \frac{\mathrm{d}\bar{T}_{\mathrm{S}}}{\mathrm{d}z} = 0,$$

$$\bar{T}_{\mathrm{S}}(0) = 0, \quad k\frac{\mathrm{d}\bar{T}_{\mathrm{S}}}{\mathrm{d}z}(0) = \frac{\mathrm{d}\bar{T}_{\mathrm{L}}}{\mathrm{d}z}(0) + \mathscr{L}\rho^{-1}.$$

So

$$\bar{T}_{\mathrm{S}} = \kappa\rho G_{\mathrm{S}}\{1 - \mathrm{e}^{-z/\kappa\rho}\}, \tag{2.12}$$

where $G_{\mathrm{S}} = (\mathscr{L} + \rho)/(k\rho)$ is the solid temperature gradient at the interface.

Now that we have a steady, basic-state solution, we formulate the standard linear stability problem. The perturbations of the basic state are defined as

$$T_{\mathrm{S}} = \bar{T}_{\mathrm{S}} + T'_{\mathrm{S}}, \quad T_{\mathrm{L}} = \bar{T}_{\mathrm{L}} + T'_{\mathrm{L}}, \tag{2.13a,b}$$

$$\boldsymbol{v} = \bar{\boldsymbol{v}} + \boldsymbol{v}', \quad p = \bar{p} + p', \tag{2.13c,d}$$

$$\mu = \bar{\mu} + \mu', \quad \eta = \eta'. \tag{2.13e,f}$$

Substituting these expressions into the governing equations and linearizing in the disturbance quantities yields:

for the solid,
$$\frac{\partial T'_{\mathrm{S}}}{\partial t}-\frac{1}{\rho}\frac{\partial T'_{\mathrm{S}}}{\partial z}=\kappa\nabla^2 T'_{\mathrm{S}}; \tag{2.14}$$

for the liquid,
$$\frac{\partial T'_{\mathrm{L}}}{\partial t}-\frac{\partial T'_{\mathrm{L}}}{\partial z}+\frac{\mathrm{d}\bar{T}_{\mathrm{L}}}{\mathrm{d}z}w'=\nabla^2 T'_{\mathrm{L}}, \tag{2.15a}$$

$$P^{-1}\left\{\frac{\partial \boldsymbol{v}'}{\partial t}-\frac{\partial \boldsymbol{v}'}{\partial z}\right\}=-\nabla p'-RT'_{\mathrm{L}}\boldsymbol{e}_3+\nabla\cdot(\bar{\mu}\boldsymbol{D}'), \tag{2.15b}$$

$$\nabla\cdot\boldsymbol{v}'=0, \tag{2.15c}$$

$$D'_{ij}=v'_{i,j}+v'_{j,i}; \tag{2.15d}$$

boundary conditions at $z=0$,
$$T'_{\mathrm{S}}=T'_{\mathrm{L}}+\eta'\left\{\frac{\mathrm{d}\bar{T}_{\mathrm{L}}}{\mathrm{d}z}-\frac{\mathrm{d}\bar{T}_{\mathrm{L}}}{\mathrm{d}z}\right\}, \tag{2.16a}$$

$$T'_{\mathrm{L}}=-\frac{\mathrm{d}\bar{T}_{\mathrm{L}}}{\mathrm{d}z}\eta'+\Gamma K', \tag{2.16b}$$

$$k\frac{\partial T'_{\mathrm{S}}}{\partial z}-\frac{\partial T'_{\mathrm{L}}}{\partial z}=\mathscr{L}\eta'_t-\eta'\left\{k\frac{\mathrm{d}^2\bar{T}_{\mathrm{S}}}{\mathrm{d}z^2}-\frac{\mathrm{d}^2\bar{T}_{\mathrm{L}}}{\mathrm{d}z^2}\right\}, \tag{2.16c}$$

$$u'=(1-\rho^{-1})\eta'_x,\quad v'=(1-\rho^{-1})\eta'_y,\quad w'=(1-\rho)\eta'_t; \tag{2.16d,e,f}$$

boundary conditions at $z=\infty$,
$$T'_{\mathrm{L}}=0,\quad |\boldsymbol{v}'|<\infty; \tag{2.17a,b}$$

and the boundary condition at $z=-\infty$,
$$T'_{\mathrm{S}}=0. \tag{2.18}$$

We eliminate the pressure from the liquid momentum equation by taking the curl of this equation twice. In addition, we attempt to find a solution of these disturbance equations using normal modes. Thus,
$$\{T'_{\mathrm{S}},T'_{\mathrm{L}},w',\eta'\}=\{\hat{T}_{\mathrm{S}}(z),\hat{T}_{\mathrm{L}}(z),\hat{w}(z),\hat{\eta}\}\,\mathrm{e}^{\sigma t}H(x,y), \tag{2.19}$$

where $\sigma=\sigma_{\mathrm{r}}+\mathrm{i}\sigma_{\mathrm{i}}$ contains σ_{r}, the growth rate, and σ_{i}, the frequency of the disturbance, and
$$\nabla_1^2 H+a^2H=0, \tag{2.20a}$$

$$\nabla_1^2=\frac{\partial^2}{\partial x^2}+\frac{\partial^2}{\partial y^2}, \tag{2.20b}$$

where H is the form of the disturbance mode and a is the wavenumber.

This results in the following normal-mode disturbance equations:

for the solid,
$$\sigma\hat{T}_{\mathrm{S}}-\rho^{-1}\mathrm{D}\hat{T}_{\mathrm{S}}=\kappa(\mathrm{D}^2-a^2)\hat{T}_{\mathrm{S}}; \tag{2.21}$$

for the liquid,
$$\sigma\hat{T}_{\mathrm{L}}-\mathrm{D}\hat{T}_{\mathrm{L}}+\frac{\mathrm{d}\bar{T}_{\mathrm{L}}}{\mathrm{d}z}\hat{w}=(\mathrm{D}^2-a^2)\hat{T}_{\mathrm{L}}, \tag{2.22a}$$

$$\{\bar{\mu}(\mathrm{D}^2-a^2)+P^{-1}(\mathrm{D}-\sigma)+2\bar{\mu}_z\,\mathrm{D}\}\{\mathrm{D}^2-a^2\}\hat{w}+\bar{\mu}_{zz}(\mathrm{D}^2+a^2)\hat{w}+Ra^2\hat{T}_{\mathrm{L}}=0; \tag{2.22b}$$

boundary conditions at $z = 0$,

$$\hat{T}_S = \hat{T}_L + \hat{\eta}\left\{\frac{d\bar{T}_L}{dz} - \frac{d\bar{T}_S}{dz}\right\}, \tag{2.23a}$$

$$\hat{T}_L = -\frac{d\bar{T}_L}{dz}\hat{\eta} - a^2\Gamma\hat{\eta}, \tag{2.23b}$$

$$k\mathrm{D}\hat{T}_S - \mathrm{D}\hat{T}_L = \mathscr{L}\sigma\hat{\eta} - \hat{\eta}\left\{k\frac{d^2\bar{T}_S}{dz^2} - \frac{d^2\bar{T}_L}{dz^2}\right\}, \tag{2.23c}$$

$$\hat{w} = \sigma(1-\rho)\hat{\eta}, \tag{2.23d}$$

$$\mathrm{D}\hat{w} = a^2(1-\rho^{-1})\hat{\eta}; \tag{2.23e}$$

boundary conditions at $z = \infty$,

$$\hat{T}_L = 0, \quad \hat{w} < \infty, \quad \mathrm{D}\hat{w} < \infty; \tag{2.24a,b,c}$$

and the boundary condition at $z = -\infty$,

$$\hat{T}_S = 0. \tag{2.25}$$

Here, $\mathrm{D} \equiv \mathrm{d}/\mathrm{d}z$.

The solid energy equation (2.21) together with the boundary conditions (2.23*a*), (2.25) and (2.23*b*) can be solved directly. We find

$$\hat{T}_S = A_S e^{mz}, \tag{2.26a}$$

$$m = \frac{-\rho^{-1} + [\rho^{-2} + 4\kappa(\sigma + \kappa a^2)]^{\frac{1}{2}}}{2\kappa}, \tag{2.26b}$$

$$A_S = -(G_S + a^2\Gamma)\hat{\eta}. \tag{2.26c}$$

This solution for $\hat{T}_S$ can now be used in the last boundary condition (2.23*c*) for the liquid temperature. This yields the final set of equations that must be solved

$$\{\bar{\mu}(\mathrm{D}^2 - a^2) + 2\bar{\mu}_z\mathrm{D} + P^{-1}(\mathrm{D} - \sigma)\}\{\mathrm{D}^2 - a^2\}\hat{w} + \bar{\mu}_{zz}(\mathrm{D}^2 + a^2)\hat{w} + Ra^2\hat{T}_L = 0, \tag{2.27a}$$

$$(\mathrm{D}^2 - a^2 + \mathrm{D} - \sigma)\hat{T}_L - \frac{d\bar{T}_L}{dz}\hat{w} = 0, \tag{2.27b}$$

$$\left.\begin{aligned} \mathrm{D}\hat{T}_L + B\hat{T}_L &= 0 \\ \hat{w} &= \sigma(1-\rho)\hat{\eta} \\ \mathrm{D}\hat{w} &= a^2(1-\rho^{-1})\hat{\eta} \end{aligned}\right\} \quad \text{on } z = 0, \tag{2.27c,d,e}$$

$$\hat{T}_L = 0, \quad \hat{w} < \infty, \quad \mathrm{D}\hat{w} < \infty \quad \text{on } z = \infty. \tag{2.27f,g,h}$$

Here

$$\hat{\eta} = \frac{-\hat{T}_L(0)}{1 + a^2\Gamma}, \tag{2.27i}$$

$$B = \frac{1 - kG_S\{m + 1/(\rho\kappa)\} - mka^2\Gamma - \mathscr{L}\sigma}{1 + a^2\Gamma}, \tag{2.27j}$$

$$kG_S = 1 + \mathscr{L}\rho^{-1}, \tag{2.27k}$$

$$m = \frac{-1 + [1 + 4\kappa\rho^2(\kappa a^2 + \sigma)]^{\frac{1}{2}}}{2\kappa\rho}, \tag{2.27l}$$

and
$$\bar{T}_{\mathrm{L}} = 1 - \mathrm{e}^{-z}, \quad \bar{\mu} = \bar{\mu}(\bar{T}_{\mathrm{L}}). \tag{2.27m,n}$$

To proceed with the solution of this set of equations we need to propose a viscosity law. Following Stengel *et al.* (1982), Morris & Canright (1984) and Quareni *et al.* (1985), we shall use an exponential viscosity variation of dimensional form

$$\mu^* = \mu_\infty \exp\{-c(T - T_\infty)\}. \tag{2.28}$$

Here, we have adjusted the constants so that $\mu^*(T_\infty) = \mu_\infty$. Substituting the appropriate scaling for the viscosity and the liquid temperature we obtain

$$\mu = \exp\{-\lambda(T_{\mathrm{L}} - 1)\}, \tag{2.29}$$

where $\lambda = c\Delta T$ is a measure of the viscosity contrast in the liquid. For the basic state, we find
$$\bar{\mu} = \exp\{-\lambda(\bar{T}_{\mathrm{L}} - 1)\} = \exp\{\lambda \exp(-z)\}. \tag{2.30}$$

Thus, $\bar{\mu}(0) = \mathrm{e}^{\lambda}$ and
$$\lambda = \ln \bar{\mu}(0) = \ln\left(\frac{\mu_{\mathrm{I}}}{\mu_\infty}\right), \tag{2.31}$$

is the natural logarithm of the viscosity ratio between the interface and the isothermal bulk liquid. Here, μ_{I} is the viscosity at the solidifying interface.

3. Method of solution

As shown in the previous section we have nine dimensionless parameters characterizing this problem. However, only four, P, R, a and λ, appear in the differential equations, one more, ρ, appears in the velocity boundary conditions, and all the rest together with the wavenumber appear in the Biot number B.

To simplify our calculations, we choose $\kappa = 1$, $\rho = 1$, $\Gamma = \infty$, and $\mathscr{L} = 0$. This leaves us with the five dimensionless groups P, R, a, k and λ. With $\Gamma = \infty$, $B = -mk$ and by varying k from 0 to ∞ we can vary B over the range 0 to $-\infty$. This will give us an indication of the effect of the parameters that make up B, but which, for simplicity, we have fixed.

Note also that when $k \to \infty$, we obtain the same simplification in the boundary conditions (2.27*d*,*e*) since $\hat{\eta} \to 0$. Thus, the problem becomes independent of the parameters κ, ρ, Γ and $\mathscr{L}$, and our analysis is valid with no further parameter restrictions.

In general, one cannot prove that the principle of exchange of stabilities is valid for this problem because of the appearance of the odd derivatives in (2.27*a*) and (2.27*b*). However, we have solved these equations with a finite-difference scheme which showed that the principle is true near the critical points of the linear theory by verifying that $\sigma_{\mathrm{i}} = 0$ at the minimum of the neutral curve. These finite-difference calculations were done for both $B = 0$ and $-\infty$ with $\lambda = 0$ and $P = 0.01$ and 10^6, and with $\lambda = 10$ and $P = 0.01$ and 1.

The remaining eigenvalue calculations were done using the routine SUPORT, written by Scott & Watts (1975, 1977). Briefly, this code uses a variable step-size, Runge–Kutta integrator coupled with a superposition algorithm to solve the boundary-value problem. Orthonormalization is also included to overcome any stiffness problems associated with the differential system at large values of the Rayleigh number. The eigenvalue part of the calculation is based on a secant-method iteration algorithm written by the author.

The only remaining subtlety in the numerical solution is the handling of the boundary conditions at infinity. New conditions were developed asymptotically by solving the governing system (2.27) in the limit of large z, for which $\bar{\mu} \to 1$ and $\mathrm{d}\bar{T}_\mathrm{L}/\mathrm{d}z \to 0$. Our equations become

$$(\mathrm{D}^2 - a^2 + P^{-1}\mathrm{D})(\mathrm{D}^2 - a^2)\,\hat{w} + Ra^2\hat{T}_\mathrm{L} = 0,$$

$$(\mathrm{D}^2 - a^2 + \mathrm{D})\,\hat{T}_\mathrm{L} = 0,$$

where the principle of exchange of stabilities has been used. These equations can be solved exactly for $\hat{T}_\mathrm{L}$ and $\hat{w}$. We find that

$$\hat{w}, \hat{T}_\mathrm{L} \sim \mathrm{e}^{-sz},$$

$$s = \tfrac{1}{2}[1 + (1 + 4a^2)^{\frac{1}{2}}].$$

From these relations, we pose the boundary conditions

$$\mathrm{D}\hat{T}_\mathrm{L} + s\hat{T}_\mathrm{L} = 0, \quad \mathrm{D}\hat{w} + s\hat{w} = 0, \quad \mathrm{D}^3\hat{w} + s\mathrm{D}^2\hat{w} = 0, \tag{3.1a–c}$$

on $z = z_{\max}$, where $z_{\max}$ is some suitably large number.

The advantage of using these asymptotic boundary conditions as opposed to the simpler set of conditions, i.e. $\hat{T}_\mathrm{L} = \hat{w} = \mathrm{D}\hat{w} = 0$ on $z = z_{\max}$, is that the previous set of conditions yields much better accuracy for the same value of $z_{\max}$ and the solution appears to be much less sensitive to the value of $z_{\max}$, provided that it is large enough.

4. Results

Representative neutral curves are shown in figure 2 for $k = 1$, $P = \infty$ and 0.01, and $\lambda = 0$ and 10. The curves display a clear minimum, or critical point, at a relatively small value of a. The small circle on curve (c) indicates that the neutral curve ceases to exist beyond this point. Presumably, the instability becomes time periodic for these larger wavenumbers. Future work will be concerned with the study of these unsteady modes since it is possible for one of them to become the critical mode of instability in some parameter range. The cross on curves (b, d) indicates a failure of the numerical algorithm to calculate the neutral point for this value of the wavenumber due to overflow errors caused by the exponentials in the governing equations. This problem can be overcome through the use of a coordinate transformation as employed by Hurle *et al.* (1983). We shall not pursue this matter since the error occurs well past the critical point and does not affect our results.

The remaining data curves are plots of the minimum Rayleigh umber R_c and the wavenumber at this minimum a_c versus the parameters P, λ and k. Figure 3(a, b) shows the dependence of R_c and a_c on P with $\lambda = 0$ and for $k = 0$, 1 and ∞. This value of λ represents the constant-viscosity case. Note the monotonic decrease in R_c and a_c with increasing P. For small P, the curves indicate that $R_\mathrm{c} \sim P^{-1}$. These curves also show that the influence of k is small. At $P = 0.01$ the difference in R_c from $k = 0$ to $k = \infty$ is 22% while at $P = \infty$ it is 14%. The $k = 1$ curve for the Rayleigh number is almost indistinguishable from the $k = 0$ curve so it was not plotted. The wavenumber a_c shows only a slight variation with k over this Prandtl-number range. The total change is never more than -0.01 to $+0.02$ with respect to the value when $k = 0$.

We can compare these results for R_c and a_c directly with the results of Hurle *et al.* (1983). Their governing equations (5) and (6) for the instability of a binary alloy

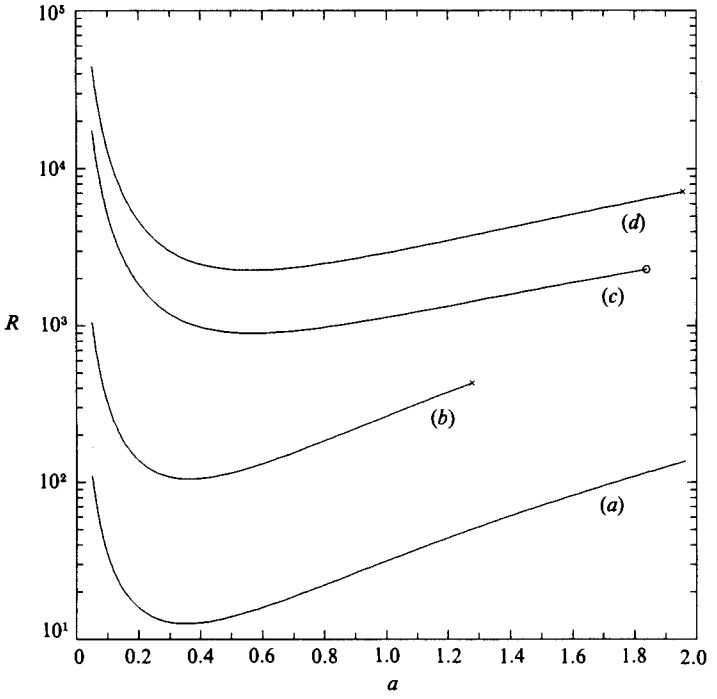

FIGURE 2. Neutral curves with $k = 1$ and for (*a*) $P = \infty$, $\lambda = 0$, (*b*) $P = \infty$, $\lambda = 10$; × indicates that the curve could not be computed beyond this point owing to numerical overflow errors, (*c*) $P = 0.01$, $\lambda = 0$; ○ indicates the neutral curve ceases to exist beyond this point for $\sigma_i = 0$, and (*d*) $P = 0.01$, $\lambda = 10$; × indicates that the curve could not be computed beyond this point owing to numerical overflow errors.

during directional solidification is exactly the same as our system if we set $k = 0$ and use a value of their partition coefficient equal to one. We find that R_c differs by at most 1.6% and a_c agrees to two significant figures.

Figure 3 (*c*, *d*) shows curves for the dependence of R_c and a_c on P when $\lambda = 15$. The same trends are apparent with only a larger value of R_c. Here, the difference in R_c between $k = 0$ and $k = \infty$ for $P = 0.01$ is 3% and for $P = \infty$ it is only 1%. Such a small difference is indistinguishable on the plot, so only the $k = 1$ curve was plotted. From these results, we see that the influence of k on R_c for these large values of λ has been significantly reduced. Also, the P^{-1} dependence of R_c for small P has been destroyed, at least for these values of P. We calculate that $R_c \sim P^{-0.85}$ at $P = 0.01$, but it does not seem that a limiting value of the exponent has yet been obtained. The magnitude of the changes in a_c with k over the full Prandtl-number range is the same as before.

Figure 3 (*a–d*) also shows that R_c and a_c approach constant values for $P \to \infty$. These values are listed in table 1 for $\lambda = 0$ and 15.

The influence of the parameter λ on R_c with $k = 0$ and $k = \infty$ and for two values of P is shown in figure 4 (*a*, *b*). Here, we can clearly see the diminishing influence of the parameter k as λ increases for both values of P. Also note that R_c increases monotonically and eventually becomes linear with λ for λ greater than about four when $P = \infty$ and for λ greater than about eight when $P = 0.01$. The right-hand scale in figure 3 (*c*) shows the behaviour of $\tilde{R}_c = R_c/\lambda$ versus P with $k = 1$ in this limit of $\lambda \to \infty$. Numerical values of $\tilde{R}_c$ in this limit are listed in table 2.

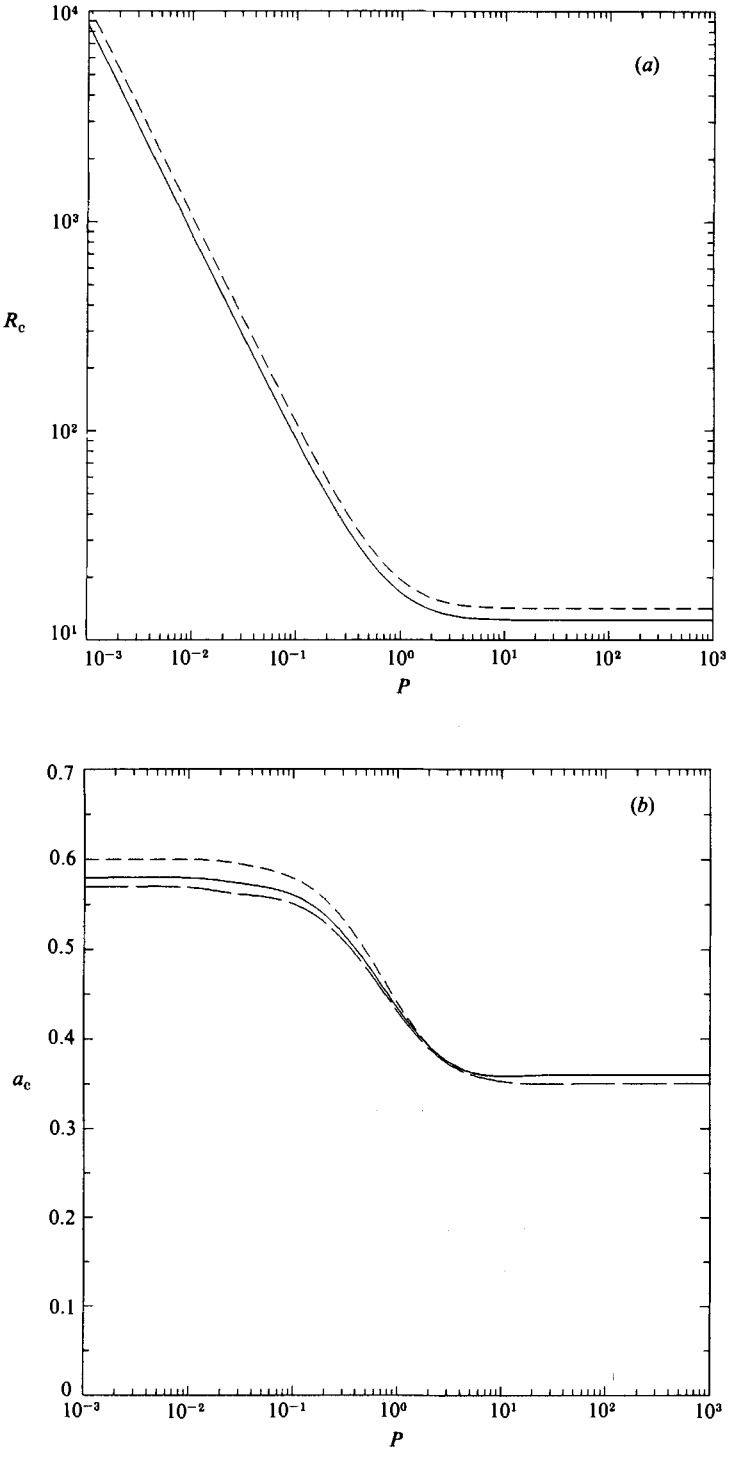

FIGURE 3(*a*,*b*). For caption see facing page.

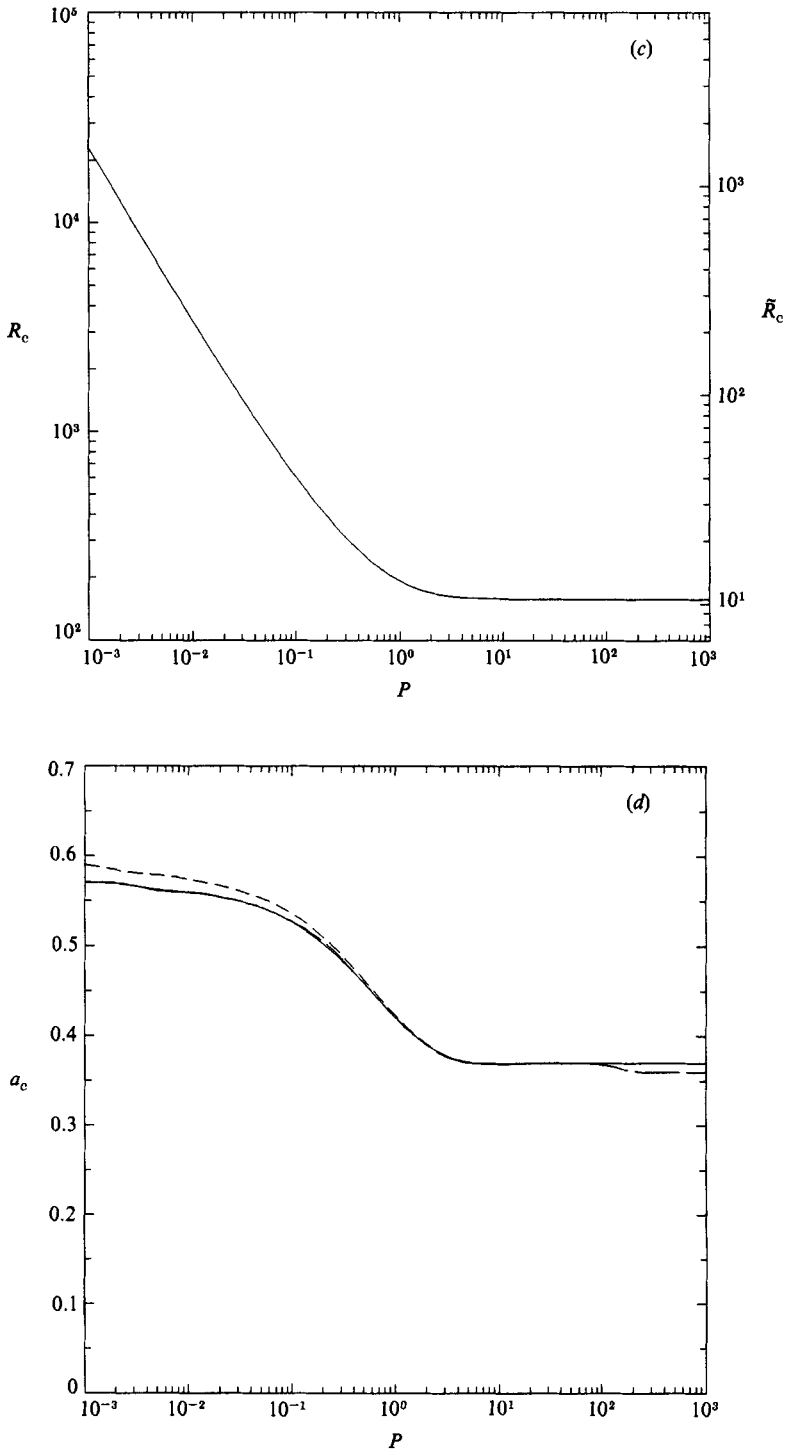

FIGURE 3. The influence of the Prandtl number on (*a*) R_c for $\lambda = 0$; ——, $k = 0$; – – –, $k = \infty$; (*b*) a_c for $\lambda = 0$; ——, $k = 0$; ——, $k = 1$; – – – –, $k = \infty$; (*c*) R_c for $\lambda = 15$ and $k = 1$ on the left-hand scale and $\tilde{R}_c$ for $k = 1$ on the right-hand scale; and (*d*) a_c for $\lambda = 15$; ——, $k = 0$; ——, $k = 1$; – – – –, $k = \infty$.

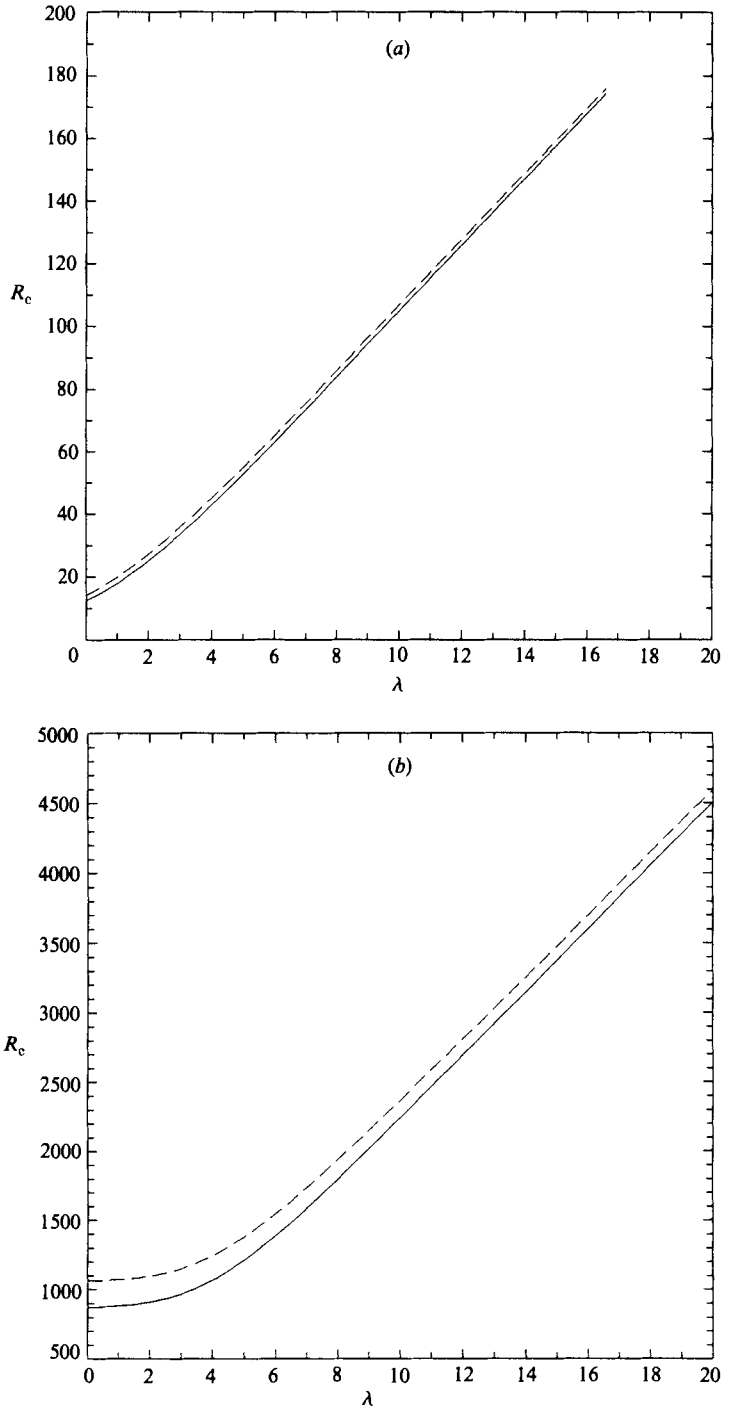

FIGURE 4. The influence of the parameter λ on R_c for (*a*) $P = \infty$; ——, $k = 0$; – – –, $k = \infty$; and (*b*) $P = 0.01$; ——, $k = 0$; – – –, $k = \infty$.

	R_c			a_c		
	$k=0$	1	∞	$k=0$	1	∞
$\lambda=0$	12.46	12.60	14.16	0.36	0.35	0.36
$\lambda=15$	157.4	157.5	159.1	0.37	0.36	0.37

TABLE 1. Asymptotic values of the critical Rayleigh number R_c and the critical wavenumber a_c as $P\to\infty$ for $\lambda=0$ and 15 and $k=0$, 1 and ∞

	$\tilde{R}_c$			a_c		
	$k=0$	1	∞	$k=0$	1	∞
$P=\infty$	10.49	10.50	10.59	0.37	0.36	0.37
$P=0.01$	225.3	226.0	229.7	0.56	0.56	0.57

TABLE 2. Asymptotic values of the critical Rayleigh number $\tilde{R}_c$ and the critical wavenumber a_c as $\lambda\to\infty$ for $P=\infty$ and 0.01 and $k=0$, 1 and ∞

The variation of a_c with λ for $P=\infty$ shows an increase of at most 0.01 for the full range of λ and the three values of k considered. At $P=0.01$, a_c decreased by at most 0.03 through the full range of λ. The limiting values of a_c for $\lambda\to\infty$ are also shown in table 2.

5. Discussion

The primary result of interest is the fact that $R_c\sim\lambda$ for large λ. This result implies that a simple rescaling of the problem is needed. The required scaling starts with the translation $z=\ln\lambda+\xi$ which renders the function $\bar{\mu}=e^f$, with $f=\lambda e^{-z}$ independent of λ, i.e. f becomes $e^{-\xi}$. Using this change of variables and the scalings $\tilde{w}=\lambda^{-1}\hat{w}$ and $\tilde{R}=\lambda^{-1}R$ the governing equations (2.27) with $\rho=1$ become

$$\{D^2-a^2-2fD+e^{-f}P^{-1}D\}\{D^2-a^2\}\tilde{w}+f(1+f)(D^2+a^2)\tilde{w}+e^{-f}a^2\tilde{R}\hat{T}_L=0, \quad (5.1a)$$

$$\{D^2+D-a^2\}\hat{T}_L-f\tilde{w}=0, \quad (5.1b)$$

$$\tilde{w}=D\tilde{w}=0, \quad D\hat{T}_L+B\hat{T}_L=0 \quad \text{on } \xi=-\ln\lambda, \quad (5.1c,d,e)$$

$$\hat{T}_L=\tilde{w}=D\tilde{w}=0 \quad \text{on } \xi=\infty. \quad (5.1f,g,h)$$

In these equations, λ only appears in the location of the upper boundary condition. In the limit of $\lambda\to\infty$, the equations become entirely independent of λ. Thus, both R and $\hat{w}$ scale linearly with λ for large λ, in total agreement with our computations.

The physical interpretation of this scaling can be seen in figure 5(*a*, *b*) which shows contour plots for the streamlines of two-dimensional convection rolls with $k=1$, $P=\infty$ and $\lambda=0$ and 15. The dotted line in figure 5(*b*) is the position $z_0=\ln\lambda$. Note that the region $0<z<z_0$ in figure 5(*b*) is practically motionless. This clearly illustrates a stagnant layer composed of fluid with the largest viscosity in agreement with the results of Stengel *et al.* (1982) and Jaupart & Parsons (1985) as discussed earlier. The appropriate temperature scale for the convecting region between $z=z_0$

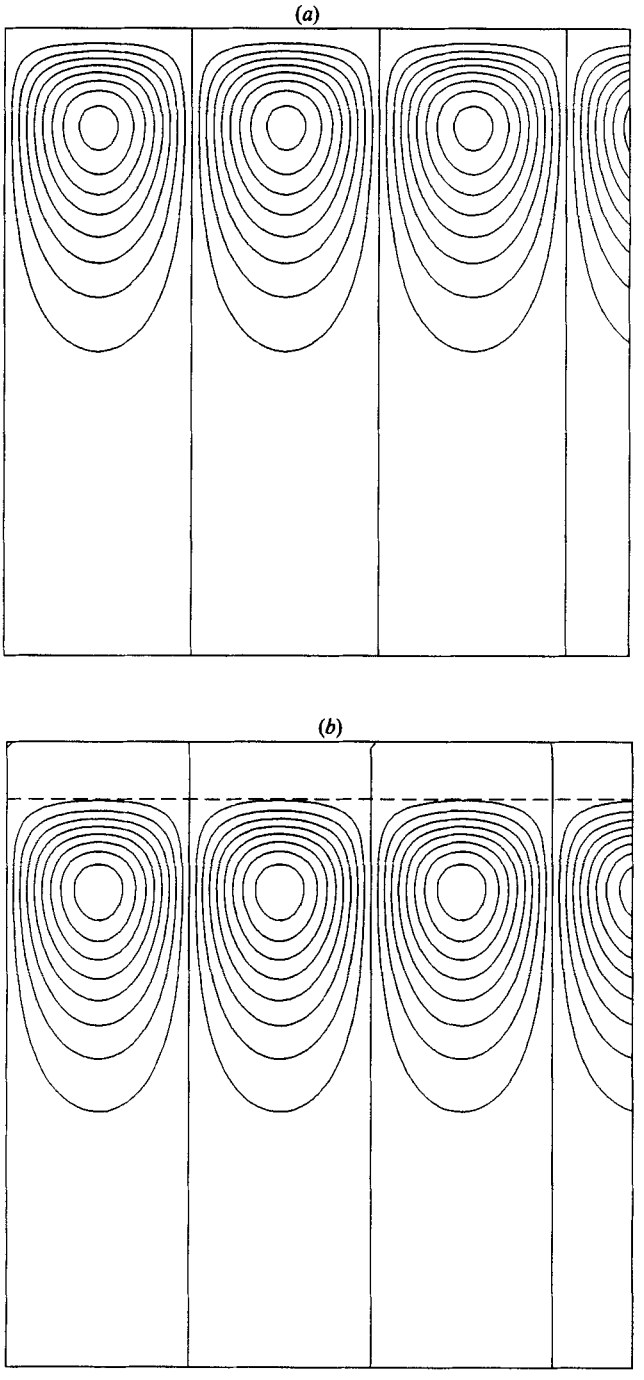

FIGURE 5. The streamlines of two-dimensional convective rolls for $k = 1$, $P = \infty$ and (*a*) $\lambda = 0$, and (*b*) $\lambda = 15$. Both plots cover a non-dimensional size of 30×30. The dashed line in (*b*) marks the position $z_0 = \ln \lambda$, the extent of the stagnant layer.

and $z = \infty$ in this limit of large λ is $\Delta T_0 = \lambda^{-1}\Delta T$, which represents the temperature difference across this convecting region. The Rayleigh number becomes

$$R = \frac{g\beta\Delta T\kappa_L^2}{\nu_\infty V^3} = \lambda\frac{g\beta\Delta T_0\kappa_L^2}{\nu_\infty V^3} = \lambda\tilde{R}, \tag{5.2}$$

exactly the result of our previous mathematical scaling argument. Thus, in the limit of large λ, the thickness of the stagnant layer is approximately $\ln\lambda$ and the Rayleigh number scaled on the temperature difference across the convecting region becomes constant. Note also that the viscosity varies by only a factor of e across this convecting region.

We can also derive this scaling result directly using an appropriate definition of a local Rayleigh number. Considering that convection in these systems with large viscosity variations always seems to occur in a sublayer near the region of smallest viscosity, we define a local Rayleigh number R_z based on convection in a sublayer between the position z and infinity. Using the temperature difference in this sublayer and the viscosity at z, we find that $R_z = R\exp\{-z-\lambda\exp(-z)\}$, where R is the original Rayleigh number. When convection occurs, it must first occur in that sublayer with the largest possible value of R_z and only when that R_z exceeds a certain critical value. The maximum value of R_z occurs at $z = z_{\max}$ defined by the equation

$$\frac{\mathrm{d}R_z}{\mathrm{d}z} = R_z\{-1+\lambda\,\mathrm{e}^{-z_{\max}}\} = 0. \tag{5.3}$$

This yields

$$z_{\max} = \ln\lambda, \quad R_z|_{\max} = \frac{\lambda^{-1}R}{\mathrm{e}}. \tag{5.4a,b}$$

Thus, the convecting region lies between $z = \ln\lambda$ and $z = \infty$. Above this sublayer, there is a stagnant layer of thickness $\ln\lambda$ which shields the convecting region from the effects of the upper interface. When λ is large enough, this stagnant layer completely shields the convecting zone and the critical value of $R_z|_{\max}$ becomes constant. Thus, for large λ, R becomes linear in λ as we have seen before. The factor of e in (5.4*b*) is just the difference between the viscosity at the top and at the bottom of the sublayer.

Figures 3 and 4 from the previous section indicate that the influence of the parameter k is fairly weak, especially as $\lambda\to\infty$. This behaviour is easily explained by considering the mechanism of the instability. Following Chandrasekhar (1961), we construct the following energetics equation for the system:

$$\frac{\mathrm{d}\mathscr{E}}{\mathrm{d}t} = \mathscr{I}+\mathscr{S}-\mathscr{D}, \tag{5.5}$$

where $\mathscr{E}$ is the mechanical and thermal energy in the convection motion over one wavelength, $\mathscr{I}$ is the potential energy, $\mathscr{S}$ is the energy lost or gained by conduction through the solidifying interface and $\mathscr{D}$ is the energy dissipation in the system due to viscous and thermal effects.

In our system, the main source of energy for the instability is the release of potential energy when a hot fluid particle rises to a colder position. This energy is represented by the integral

$$\mathscr{I} = -\int_0^\infty (Ra^2+\bar{T}_z)\,\hat{w}\hat{T}\,\mathrm{d}z.$$

The parameter k is part of the thermal boundary condition and so changes in k primarily affect the temperature field. In figure 6(*a*), we show the magnitudes of the temperature and the vertical velocity eigenfunctions for $P = \infty$, $\lambda = 0$ and $k = 0$ and ∞ normalized on the maximum value of the vertical velocity. The Rayleigh number and wavenumber are set at the critical values for $k = 0$. Since the temperature shown is the negative of the actual temperature in the system, the primary change when k is varied is an increase in the temperature near the solidifying boundary. This results in a decrease in the potential energy liberated during the motion which stabilizes the system, i.e. R_c increases as k is increased.

Note also that the change in the temperature is confined to a region near the solidifying boundary. At large values of λ, this region becomes stagnant, i.e. $\hat{w}$ also decreases. This results in a smaller change in the integral $\mathscr{I}$ and a decrease in the effect of k on R_c as we have shown. Figure 6(*b*) displays this behaviour in the eigenfunction for $P = \infty$ and $\lambda = 5$.

By varying the parameter k from 0 to ∞ we have in effect studied the influence of the Biot number over the range 0 to $-\infty$. This gives us some indication of the effect of the parameters Γ, $\mathscr{L}$ and κ which make up the Biot number, but which we initially fixed. We can conclude from our results that the effect on R_c represented by these parameters, i.e. interface deflection, latent heat and conduction at the interface, is also weak, especially at large values of λ.

Figures 3 and 4 show a very significant increase in the critical Rayleigh number as P is decreased. This is explained by considering figure 7(*a*). Here, we see the magnitudes of the eigenfunctions for temperature and vertical velocity for $k = 1$, $\lambda = 0$ and $P = \infty$ and 1 with a normalization based on the temperature at the interface. The Rayleigh number and wavenumber are set at the critical values for $P = \infty$. For the lower value of P, the vertical velocity is substantially reduced. This is due to inertial effects in that for a given temperature perturbation of a fluid particle, the resulting buoyancy force must balance both the acceleration and the viscous forces on the particle. This decreases the magnitude of the vertical velocity as shown, and consequently the amount of potential energy released is also decreased. Thus, the system becomes more stable as P decreases and so R_c increases. Figure 7(*b*) shows the eigenfunctions for $\lambda = 15$ and $P = \infty$ and 1. Note that the same effect occurs since it is associated with the bulk fluid. This is in contrast to the effects of the parameter k which is just an interfacial effect.

The critical Rayleigh numbers calculated in this study are very small compared with those from the classical studies of finite layers. This is due to our use of the thermal-diffusion lengthscale $L_s = \kappa_L/V$. The classical studies used a lengthscale based on the layer thickness over which the temperature difference is imposed. To compare our results to these studies, we define a new lengthscale L_s^* as the distance over which the temperature difference is 99% of the total temperature difference available for convection. This definition results in the relation $L_s^* = (2 \ln 10) L_s$ for both the constant- and variable-viscosity cases. With this new lengthscale, we obtain a Rayleigh number $R^* = (2 \ln 10)^3 \mathrm{R} = 97.66\mathrm{R}$ and a wavenumber $a^* = (2 \ln 10)\, a = 4.605a$. Table 3 lists R_c^* and a_c^* for $P = \infty$ and $\lambda = 0$ and ∞. Note that the value of R_c^* is now about 1000–1400 and a_c^* is approximately 1.6–1.7. These values are now of the same order of magnitude as the classical values of $R_c = 1100.65$ and $a_c = 2.682$ for a rigid free layer with constant-temperature boundary conditions (Chandrasekhar 1961).

This general agreement between the two studies does not mean that the lengthscale L_s^* fully defines this solidification problem because it does not define the

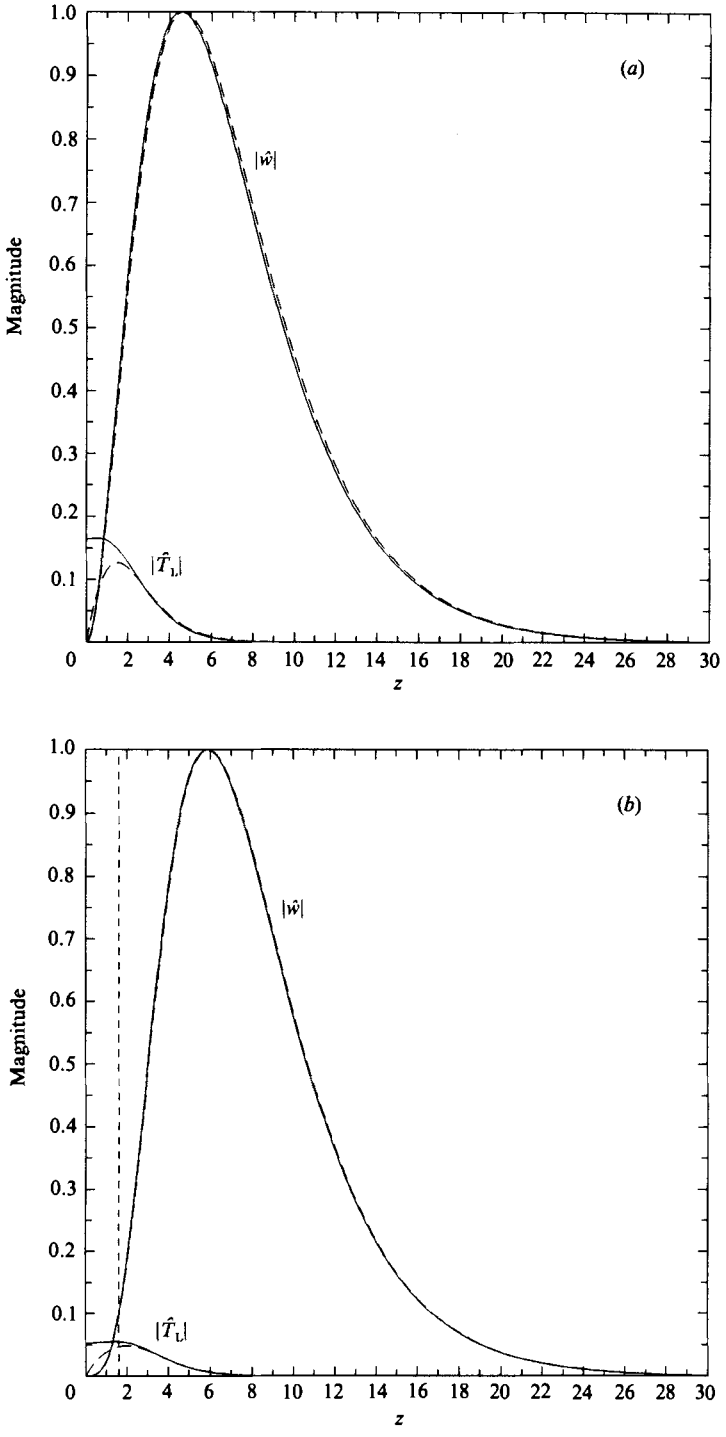

FIGURE 6. The vertical velocity and the negative of the temperature eigenfunctions with $P = \infty$ and for (*a*) $\lambda = 0$, $R = 12.46$ and $a = 0.36$ and for (*b*) $\lambda = 5$, $R = 52.77$ and $a = 0.37$. ——, $k = 0$; – – – –, $k = \infty$. The vertical dashed line marks the stagnant layer, $z_0 = \ln \lambda$.

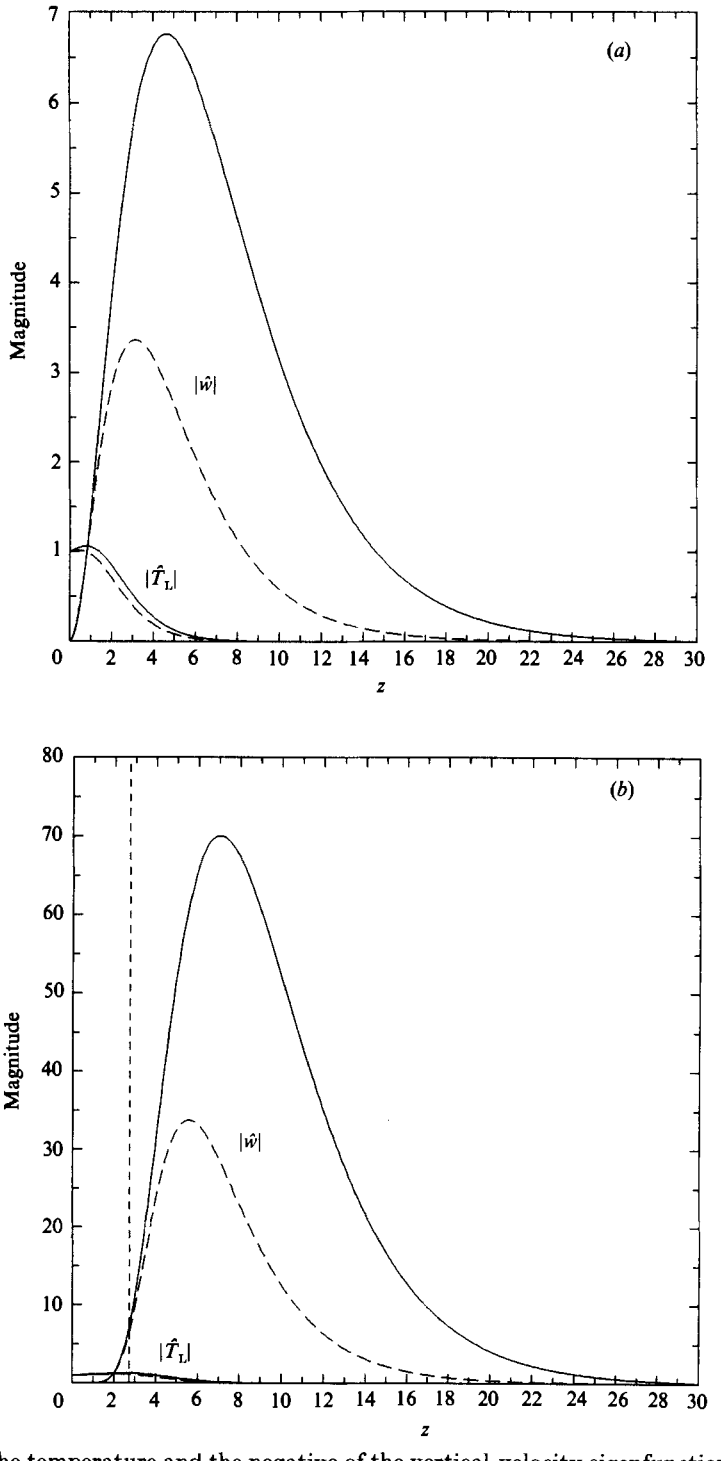

FIGURE 7. The temperature and the negative of the vertical-velocity eigenfunctions with $k = 1$ and for (*a*) $\lambda = 0$, $R = 12.60$ and $a = 0.35$, and for (*b*) $\lambda = 15$, $R = 157.5$ and $a = 0.36$. ——, $P = \infty$; – – – –, $P = 1.0$. The vertical dashed line marks the stagnant layer, $z_0 = \ln \lambda$.

	R_c^*			a_c^*		
	$k = 0$	1	∞	$k = 0$	1	∞
$\lambda = 0$	1217	1231	1383	1.66	1.61	1.66
$\lambda = \infty$	1025	1026	1034	1.70	1.66	1.70

TABLE 3. The rescaled critical Rayleigh number R_c^* and the critical wavenumber a_c^* for $P = \infty$, $\lambda = 0$ and ∞, and $k = 0$, 1 and ∞

depth of penetration of the convective rolls. As shown in figure 6, convection occurs in a region on the order of $20L_s$. This larger penetration is due to the effects of viscosity.

In applying this theory to a solidifying magma system, we shall use the following typical property values: $\beta = 5 \times 10^{-5}$ °C^{-1}, $\kappa = 10^{-2}$ cm^2/s, $\rho = 2.6$ g/cm^3, $\mu_\infty = 10^2$ g/(cm s), $\mu_I = 10^7$ g/(cm s) and a melting temperature $T_m = 1100$ °C. Relevant dimensionless groups are $P = 3850$, $k = 1$ and $\lambda = 11.5$. Given a $\Delta T = 200$ °C and using the appropriate value of $\tilde{R}_c = 10.5$ from table 2, we find that the critical velocity *below* which the system is unstable is

$$V_c = 6.0 \times 10^{-3} \text{ cm/s} = 1.9 \text{ km/yr}.$$

Since an average solidification speed for these systems may be on the order of $V = 0.01$ km/yr, we can expect the appearance of convection.

The critical velocity is reached early in the solidification of the liquid. Using the standard Stefan model of this process and ignoring latent heat (see Carslaw & Jaeger 1959), we find that the velocity of the interface is $V = q(\kappa_L/t)^{\frac{1}{2}}$, where $q = 1.01$. Thus, V_c occurs 280 s after the start of solidification. The crust is 3.4 cm thick at this point.

The thermal lengthscale associated with the above property values at the critical point is $L_s = 1.67$ cm. Other lengthscales of interest at this critical value for the solidification velocity are as follows. The length over which 99% of the total temperature difference occurs is $L_s^* = 7.7$ cm, an estimate of the stagnant-layer thickness is $L_r = L_s \ln \lambda = 4.1$ cm, and an estimate of the size of the convecting region below the stagnant layer is $L_c = 20L_s = 33.4$ cm. The thickness of a typical magma chamber may be on the order of one or several kilometers. This distance is much larger than the lengthscales in our convection process so the assumption of a semi-infinite fluid is valid. Also, from table 2 we have $a_c = 0.36$, which yields a width for the convection cell of $L_w = 14.6$ cm. The ratio $L_w/L_c = 0.44$ indicates that the cells are not quite half as wide as they are deep.

Using the average solidification velocity from above, we find that the typical value of the Rayleigh number for these systems is $\tilde{R} = 7 \times 10^7$ with a corresponding lengthscale of $L_s = 315$ cm. Since the critical Rayleigh number for this system is $\tilde{R}_c = 10.5$, we are driving the system at about 6.67×10^6 times critical. If we assume for the sake of discussion that the convection can still be characterized by its lengthscales at the critical point, we find that $L_s^* = 14.5$ m, $L_r = 7.7$ m, $L_c = 63.0$ m and $L_w = 27.5$ m. Thus, convection extends about 71 m below the solidifying interface. This distance is still much less than the kilometer-sized chamber, so the semi-infinite model may still be valid even at these extremely slow solidification velocities.

There are two relevant timescales in this study. The first, t_I, is the time rate of

change of the interface velocity V. We calculate this from the standard Stefan problem as $t_I = |V(dV/dt)^{-1}| = 2t$, where t is the time at which the velocity V occurs. The second timescale $t_G = t_s/\sigma_r$ measures the growth rate of the disturbance. Here, t_s is the diffusive timescale. At the critical velocity, $t_I = 566$ s and $t_s = 278$ s, and at the average velocity $t_I = 230$ days and $t_s = 113$ days.

For this model to be an accurate representation of a solidifying system, $t_G \ll t_I$. Using the standard Stefan model for V, we obtain $\sigma_r \gg 1/(2q)$. As with all of these quasi-steady models, the model is invalid at the critical point where $\sigma_r = 0$. However, the model does yield a qualitative description of the system, especially when the growth rate of the disturbance is much larger than about one-half.

Large Rayleigh-number convection in thin layers with constant temperature boundaries is very vigorous and large heat fluxes occur at both the top and bottom surfaces. In a solidifying magma system this may not be the case. The heat flux out of the top of the system controls the solidification velocity. In a naturally cooling system described by the standard Stefan model, the heat flux from the top and the solidification velocity decrease like $t^{-\frac{1}{2}}$. This decrease in V increases the lengthscale of the convection and so the net potential energy available for convection increases. This makes the system more unstable as we have seen. However, the resultant convection can only reduce the temperature difference in the fluid over this new lengthscale since there is no heat flux through the bottom and the heat flux through the top is limited by the solid. This reduces the net potential energy available for convection which in turn stabilizes the system. Thus, convection competes with the decreasing solidification velocity and the final result may be a gentle circulation not much different than that just past the critical point.

6. Conclusions

We have used linear stability theory to study the onset of buoyancy-driven convection during the directional solidification of a liquid with a strongly temperature-dependent viscosity and an arbitrary Prandtl number. The Rayleigh number for this system contains the lengthscale L_s defined as the ratio of the thermal diffusivity and the solidification velocity times the density ratio of the two phases. It is independent of the actual depth of the liquid and it reflects the fact that increasing the solidification velocity stabilizes the system. Typical values of the critical Rayleigh number are listed in tables 1 and 2.

For large viscosity variations, a stagnant layer forms just below the solidifying interface where the liquid becomes immobilized by its very large viscosity. The thickness of this layer is approximately $L_s \ln\lambda$, where $\lambda = \ln(\mu_I/\mu_\infty)$ is the natural logarithm of the viscosity contrast in the liquid. Convection occurs below the stagnant layer. In the limit of large viscosity variations, the critical Rayleigh number becomes linear in λ. This suggests a new temperature scaling based on the temperature difference across the convecting layer only. This rescaled Rayleigh number $\tilde{R}$ is defined in (5.2).

The theory also shows that the material properties associated with the two phases manifest themselves in a wavenumber-dependent Biot number for the solidifying interface. This causes the interface to look like a boundary of finite conductivity. However, the effect of this conductivity is small since it is purely an interfacial effect and the convection is driven by body forces in the bulk liquid. Decreasing the Biot number from zero to $-\infty$ changes the critical Rayleigh number by at most 22% for a constant-viscosity liquid. In the limit of large viscosity variations, the influence of

the solidifying boundary is shielded from the bulk liquid by the stagnant layer and so the effect of the Biot number on the critical Rayleigh number is even smaller, i.e. only 3% over this same Biot number range.

However, inertial effects, being associated with the *bulk* liquid, are very important for small Prandtl numbers of the fluid far from the interface. In this limit, $R_c \sim P^{-1}$ for the constant-viscosity case and $R_c \sim P^{-0.85}$ at $P = 0.01$ in the limit of large viscosity variations.

The critical Rayleigh number for a system with large viscosity variations is $\tilde{R}_c = 10.5$. In a typical cooling magma system, this value is exceeded when $V < 1.9$ km/yr. An average solidification velocity for such a system is about 0.01 km/yr so some form of convection is expected. The lengthscale associated with this convection at both the critical velocity and the average velocity is still much smaller than the typical thickness of a magma chamber. Thus, our model of a semi-infinite liquid is valid for studying these systems.

The above critical solidification velocity occurs early in the solidification of the magma. As the process continues, the solidification velocity and the heat flux from the system decrease. This increases the lengthscale over which temperature changes occur in the liquid thereby destabilizing the system. Convection on the other hand, being constrained by the heat-flux conditions at the system boundaries, attempts to destroy the net temperature difference across the liquid which in turn stabilizes the system. These two competing effects could result in a new equilibrium in which only a gentle circulation is present in the liquid. This is in contrast to the vigorous convection that occurs at large Rayleigh numbers in thin-liquid-layer systems with fixed temperature boundaries. Future work on this system using nonlinear techniques is needed to verify this hypothesis.

The author is very grateful to Professor Bruce D. Marsh for many interesting discussions, during which we quantified his intuitive physical understanding of the role of convection in solidifying magma systems into the model used in this study. The figures in this paper were drawn using the NCAR graphics system.

REFERENCES

BOOKER, J. R. 1976 Thermal convection with strongly temperature-dependent viscosity. *J. Fluid Mech.* **76**, 741–754.

CAROLI, B., CAROLI, C., MISBAH, C. & ROULET, B. 1985*a* Solutal convection and morphological instability in directional solidification of binary alloys. *J. Phys. Paris* **46**, 401–413.

CAROLI, B., CAROLI, C., MISBAH, C. & ROULET, B. 1985*b* Solutal convection and morphological instability in directional solidification of binary alloys. II. Effect of the density difference between the two phases. *J. Phys. Paris* **46**, 1657–1665.

CARSLAW, H. S. & JAEGER, J. C. 1959 *Conduction of Heat in Solids*. Oxford University Press.

CHANDRASEKHAR, S. 1961 *Hydrodynamic and Hydromagnetic Stability*. Dover.

CORIELL, S. R., CORDES, M. R., BOETTINGER, W. J. & SEKERKA, R. F. 1980 Convective and interfacial instabilities during unidirectional solidification of a binary alloy. *J. Cryst. Growth* **49**, 13–28.

CURRIE, I. G. 1967 The effect of heating rate on the stability of stationary fluids. *J. Fluid Mech.* **29**, 337–347.

FOSTER, T. D. 1965 Stability of a homogeneous fluid cooled uniformly from above. *Phys. Fluids* **8**, 1249–1257.

GERSHUNI, G. Z. & ZHUKHOVITSKII, E. M. 1976 *Convective Stability of Incompressible Fluids*. Jerusalem: Keter.

HOMSY, G. M. 1973 Global stability of time-dependent flows: impulsively heated or cooled fluid layers. *J. Fluid Mech.* **60**, 129–139.

HURLE, D. T. J., JAKEMAN, E. & WHEELER, A. A. 1982 Effect of solutal convection on the morphological stability of a binary alloy. *J. Cryst. Growth* **58**, 163–179.

HURLE, D. T. J., JAKEMAN, E. & WHEELER, A. A. 1983 Hydrodynamic stability of the melt during solidification of a binary alloy. *Phys. Fluids* **26**, 624–626.

JAUPART, C. & PARSONS, B. 1985 Convective instabilities in a variable viscosity fluid cooled from above. *Phys. Earth Planet. Inter.* **39**, 14–32.

JHAVERI, B. S. & HOMSY, G. M. 1982 The onset of convection in fluid layers heated rapidly in a time-dependent manner. *J. Fluid Mech.* **114**, 251–260.

MAHLER, E. G., SCHECHTER, R. S. & WISSLER, E. H. 1968 Stability of a fluid layer with time-dependent density gradients. *Phys. Fluids* **11**, 1901–1912.

MCFADDEN, G. B., REHM, R. G., CORIELL, S. R., CHUCK, W. & MORRISH, K. A. 1984 Thermosolutal convection during directional solidification. *Metall. Trans.* A **15**, 2125–2137.

MORRIS, S. & CANRIGHT, D. 1984 A boundary-layer analysis of Bénard convection in a fluid of strongly temperature-dependent viscosity. *Phys. Earth Planet. Inter.* **36**, 355–373.

MULLINS, W. W. & SEKERKA, R. F. 1964 Stability of a planar interface during solidification of a dilute binary alloy. *J. Appl. Phys.* **35**, 444–451.

NEITZEL, G. P. 1982 Onset of convection in impulsively heated or cooled fluid layers. *Phys. Fluids* **25**, 210–211.

OLIVER, D. S. & BOOKER, J. R. 1983 Planform of convection with strongly temperature-dependent viscosity. *Geophys. Astrophys. Fluid Dyn.* **27**, 73–85.

QUARENI, F., YUEN, D. A., SEWELL, G. & CHRISTENSEN, U. R. 1985 High Rayleigh number convection with strongly variable viscosity: a comprison between mean field and two-dimensional solutions. *J. Geophys. Res.* **90**, 12633–12644.

RAYLEIGH, LORD 1916 On convective currents in a horizontal layer of fluid when the higher temperature is on the under side. *Phil. Mag.* **32**, 529–546.

RICHTER, F. M., NATAF, H.-C. & DALY, S. F. 1983 Heat transfer and horizontally averaged temperature of convection with large viscosity variations. *J. Fluid Mech.* **129**, 173–192.

SCOTT, M. R. & WATTS, H. A. 1975 SUPORT – A computer code for two-point boundary-value problems via orthonormalization. *Sandia Labs, Albuquerque, NM, Rep. SAND* 75-0198.

SCOTT, M. R. & WATTS, H. A. 1977 Computational solution of linear two-point boundary-value problems via orthonormalization. *SIAM J. Numer. Anal.* **14**, 40–70.

SHAW, H. R., WRIGHT, T. L., PECK, D. L. & OKAMURA, R. 1968 The viscosity of basaltic magma: an analysis of field measurements in Makaopuhi lava lake, Hawaii. *Am. J. Sci.* **266**, 225–264.

STENGEL, K. C., OLIVER, D. S. & BOOKER, J. R. 1982 Onset of convection in a variable-viscosity fluid. *J. Fluid Mech.* **120**, 411–431.

YOUNG, G. W. & DAVIS, S. H. 1986 Directional solidification with buoyancy in systems with small segregation coefficient. *Phys. Rev.* B **34**, 3388–3396.